Fully relativistic spin-polarized LMTO calculations of the magneto-optical Kerr effect of *d* and *f* ferromagnetic materials. I. Chromium spinel chalcogenides

V. N. Antonov,* V. P. Antropov, and B. N. Harmon
Ames Laboratory, Iowa State University, Ames, Iowa 50011

A. N. Yaresko and A. Ya. Perlov
Institute of Metal Physics, 36 Vernadsky Street, 252142 Kiev, Ukraine
(Received 21 October 1998)

$CuCr_2Se_4$ is one of the few compounds that exhibits a magneto-optical (MO) Kerr angle of greater than one degree at room temperature. To better understand the origin of this effect, the MO properties of ferromagnetic $CuCr_2X_4$ (X=S, Se, Te) spinel chalcogenides are evaluated using fully relativistic local-density electronic structure calculations. Treating the $3d$ electronic states within the standard band description, excellent agreement with the measured MO spectra is obtained. The calculations are analyzed to further elucidate aspects of the Kerr rotation. [S0163-1829(99)09221-8]

I. INTRODUCTION

The magneto-optical Kerr effect (MOKE), namely the rotation of the polarization plane of linearly polarized light on reflection from magnetic solids has been known for more than a century.[1] During the past two decades interest in this effect has increased tremendously. The reason for this is twofold: first, the Kerr effect is used in modern data storage and sensor technology,[2] and second, the Kerr effect has rapidly developed into an appealing spectroscopic tool in materials research. Magneto-optical spectroscopy has contributed to an improved understanding of the electronic structure of a wide class of materials and of many basic problems ranging from surface magnetism to exchange coupling in magnetic superconductors. Over the years the Kerr spectra of many ferromagnetic materials have been investigated. An overview of the experimental data collected on the Kerr effect can be found in the review articles by Buschow,[3] Reim and Schoenes,[4] and Schoenes.[5]

The quantum mechanical understanding of the Kerr effect began as early as 1932 when Hulme[6] proposed that the Kerr effect could be attributed to spin-orbit (SO) coupling (see also Kittel[7]). The symmetry between left- and right-hand circularly polarized light is broken due to the SO coupling in a magnetic solid. This leads to different refractive indices for the two kinds of circularly polarized light, so that incident linearly polarized light is reflected with elliptical polarization, and the major elliptical axis is rotated by the so called Kerr angle from the original axis of linear polarization. The first systematic study of the frequency dependent Kerr and Faraday effects was developed by Argyres[8] and later Cooper presented a more general theory using some simplifying assumptions[9] (also see Ref. 10). The very powerful linear response techniques of Kubo[11] gave general formulas for the conductivity tensor which are being widely used now. A general theory of frequency dependent conductivity of ferromagnetic (FM) metals over a wide range of frequencies and temperatures was developed in 1968 by Kondorsky and Vediaev.[12]

The main problem afterward was the evaluation of the complicated formulas involving MO matrix elements using electronic states of the real FM system. With the tremendous increases in computational power and the concomitant progress in electronic structure methods the calculation of such matrix elements became possible, if not routine. Subsequently many earlier, simplified calculations have been shown to be inadequate, and only calculations from ''first-principles'' have provided, on the whole, a satisfactory description of the experimental results.[13] The existing difficulties stem either from problems using the local spin density approximation (LSDA) to describe the electronic structure of FM materials containing highly correlated electrons, or simply from the difficulty of dealing with very complex crystal structures. For 15 years after the work of Wang and Callaway[13] there was a lull in MO calculations until MO effects were found to be important for magnetic recording and the computational resources had advanced. Different reliable numerical schemes for the calculation of optical matrix elements and the integration over the Brillouin zone have been implemented, giving essentially identical results.[14] Prototype studies have been performed using modern methods of band theory for Fe, Co, and Ni. Following the calculations for the elemental $3d$ ferromagnets, a number of groups have evaluated the MO spectra for more interesting compounds. To show the diversity of the materials studied and to help put our own work in context, we note the following materials for which MO calculations have been performed: half-metallic FM, CrO_2, and EuO;[15] MnBi, FePt, U_3P_4;[16] UTe, USb, CeTe;[18] FePt, MnBi, Heusler alloys, US, UAsSe, $GdFe_2$ and others;[17] FePt, CeSb, Gd.[19] MO calculations have also been performed for surfaces and multilayers.[20] While the calculations showed there is good agreement between theory and experiment in case of *d*-band magnetic materials, attempts to describe MO properties of materials using the same formalism failed to create a consistent physical picture. This has been attributed to the general failure of the LSDA in describing the electronic structure of *f*-state materials ($4f$ especially). To overcome the LSDA limitations to study MO spectra a so called E^3 correction for correlations was implemented but gave inconsistent results.[18] The more consistent

LSDA+U scheme has been used to describe the Kerr angle of CeSb.[19,21] Since then several papers implementing the LSDA+U scheme for MO calculations have been published with $4f$ and $5f$ materials.[18,22]

With the above as background, we have performed calculations to evaluate the MO properties for a number of $3d$, $4f$, and $5f$ FM materials. Besides the inherent interest in the materials studied, the use of similar methods to study materials with different degrees of localized electronic states helps to establish the limitations of the LSDA approach and to identify where techniques like the LSDA+U method are needed. We have divided the work into three papers, with this, paper I, concentrating on the description of the methods and the results for the $3d$ series of chromium chalcogenides, where the LSDA approach is successfully applied. Papers II and III deal with $4f$ and $5f$ materials, respectively, and use both the LSDA and LSDA+U approaches to assess the sensitivity of the MO results to the different treatments of the correlated electrons.

II. THE DESCRIPTION OF THE STUDIED SYSTEMS

Among the compounds containing magnetic transition elements, four large classes have attracted special attention for their MO properties. These comprise spinels, garnets, orthoferrites, and Heusler alloys. The Heusler alloys NiMnSb, PdMnSb, and PtMnSb have been the subject of intensive experimental and theoretical investigations since the early 1980s.[23] The half-metallic Heusler compound PtMnSb shows the highest Kerr rotation angle of $-1.27°$ known so far for magnetic transition metal compounds and alloys at room temperature. Recent fully relativistic spin-polarized band structure calculations were able to explain the peculiarities of the MO spectra of Heusler alloys.[24]

Although the optical and MO properties of the rest of the three groups of compounds have been the subject of intensive experimental studies over last two decades, they have received less attention with energy band structure calculations partly due to rather complicated crystal structures. Spinels have the general formula $M_A^{2+}(M_B^{3+})_2X_4$,[5] where M_A^{2+} and M_B^{3+} are di- and trivalent cations, respectively (M_A=Mg, Mn, Fe, Co, Ni, Cu, Zn, Cd; M_B=Cr, Co), and X stands for a chalcogen O, S, Se, or Te. Among the transition metal spinels the copper-chromium spinels $CuCr_2X_4$ (X=S, Se, Te) play a special role. While many other chromium spinels and particularly most oxides are insulators which order antiferromagnetically, $CuCr_2S_4$, $CuCr_2Se_4$, and $CuCr_2Te_4$ are metallic and order ferromagnetically with Curie temperatures well above room temperature, i.e., $CuCr_2S_4$ (T_c=377 K), $CuCr_2Se_4$ (T_c=430 K), and $CuCr_2Te_4$ (T_c=360 K).[25] These compounds were first synthesized by Hahn *et al.*[26] in 1956, and their magnetic properties have been reported by Lotgering in 1964.[27] The metallic character and the magnetic moment of approximately 5 μ_B, per formula unit, i.e., for two Cr atoms,[25] has promoted interest to consider these compounds as promising material for MO devices.[5] The magneto-optical polar Kerr effect measurements on $CuCr_2Se_4$ single crystals between 0.55 and 5.0 eV show[28] that the Kerr ellipticity ϵ_K reaches $-1.19°$ at 0.96 eV. The figure of merit $R^{1/2}(\theta_K^2+\epsilon_K^2)^{1/2}$, where R is the optical reflectivity has a maximum value of $0.84°$ at 0.88 eV which is as high as in PtMnSb ($0.83°$ at 1.57 eV). Although $CuCr_2Se_4$ does not contain any atom with strong spin-orbit coupling (like Pt in PtMnSb), it exhibits almost the same MO properties as PtMnSb.

The electronic structure of the $CuCr_2X_4$ (X=S, Se, Te) chalcogenides was discussed in the literature[27,29–32] but no theoretical MO calculations are available for $CuCr_2X_4$. In the present work we report a detailed theoretical investigation of the optical and MO Kerr spectra of $CuCr_2S_4$, $CuCr_2Se_4$, and $CuCr_2Te_4$.

The paper is organized as follows. The theoretical framework is explained in Sec. III. Section IV presents the description of the crystal structure of the $CuCr_2X_4$ (X=S, Se, Te) compounds and the computational details. Section V is devoted to the electronic structure of the compounds calculated in the LSDA. The results are compared to previous band structure calculations and the optical and MO theoretical calculations are compared to the experimental measurements. Finally, the results are summarized in Sec. VI.

III. THEORETICAL FRAMEWORK

Using straightforward symmetry considerations it can be shown that all MO phenomena are caused by the symmetry reduction—compared to the paramagnetic state—caused by magnetic ordering.[33] Concerning optical properties this symmetry reduction only has consequences when SO coupling is considered in addition. To calculate MO properties one therefore has to account for magnetism and SO coupling at the same time when dealing with the electronic structure of the material considered. Performing corresponding band structure calculations it is normally sufficient to treat SO coupling in a perturbative way. A more rigorous scheme, however, is obtained by starting from the Dirac equation set up in the framework of relativistic spin density functional theory:[34]

$$[c\boldsymbol{\alpha}\cdot\mathbf{p}+\boldsymbol{\beta}mc^2+\boldsymbol{I}V+V_{sp}\boldsymbol{\beta}\boldsymbol{\sigma}_z]\psi_{n\mathbf{k}}=\epsilon_{n\mathbf{k}}\psi_{n\mathbf{k}}, \qquad (1)$$

with $V_{sp}(\mathbf{r})$ the spin-polarized part of the exchange-correlation potential corresponding to the z quantization axis. All other parts of the potential are contained in $V(\mathbf{r})$. The 4×4 matrices $\boldsymbol{\alpha}$, $\boldsymbol{\beta}$, and $\boldsymbol{I}$ are defined by

$$\boldsymbol{\alpha}=\begin{pmatrix}0 & \boldsymbol{\sigma}\\ \boldsymbol{\sigma} & 0\end{pmatrix},\quad \boldsymbol{\beta}=\begin{pmatrix}\mathbf{1} & 0\\ 0 & -\mathbf{1}\end{pmatrix},\quad \boldsymbol{I}=\begin{pmatrix}\mathbf{1} & 0\\ 0 & \mathbf{1}\end{pmatrix}, \qquad (2)$$

with $\boldsymbol{\sigma}$ the standard Dirac matrices, and $\mathbf{1}$ the 2×2 unit matrix.

There are quite a few band structure methods available now that are based on the above Dirac equation.[35] In the first scheme the basis functions are derived from the proper solution to the Dirac equation for the various single-site potentials.[36,37] In the second one, the basis functions are obtained initially by solving the Dirac equation without the spin-dependent term[38,39] and then this term is accounted for only in the variational step.[17,36] In spite of this approximation, the second scheme nevertheless gives results in very good agreement with the first one,[35] while being very simply implemented. We also mention the quite popular technique when SO coupling is added variationally[38] after the scalar relativistic magnetic Hamiltonian has been constructed. In

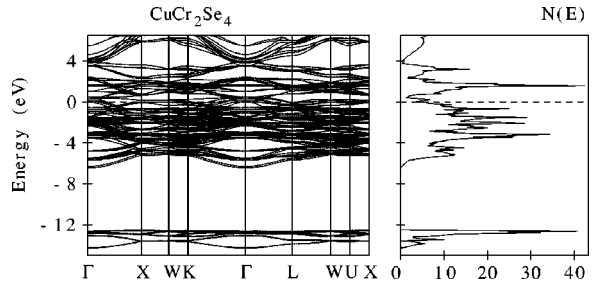

FIG. 1. Self-consistent fully relativistic, spin-polarized energy band structure and total DOS [in states/(unit cell eV)] of $CuCr_2Se_4$.

this case only the Pauli equation with SO coupling is being solved. All three techniques yield similar results.

In the polar geometry, where the z-axis is chosen to be perpendicular to the solid surface, and parallel to the magnetization direction, the expression for the Kerr angle can be obtained easily for small angles and is given by[4]

$$\theta_K(\omega)+i\varepsilon_K(\omega)=\frac{-\sigma_{xy}(\omega)}{\sigma_{xx}(\omega)\sqrt{1+\frac{4\pi i}{\omega}\sigma_{xx}(\omega)}}, \qquad (3)$$

with θ_K the Kerr rotation and ε_K the so-called Kerr ellipticity. $\sigma_{\alpha\beta}$ $(\alpha,\beta\equiv x,y,z)$ is the optical conductivity tensor, which is related to the dielectric tensor $\varepsilon_{\alpha\beta}$ through

$$\varepsilon_{\alpha\beta}(\omega)=\delta_{\alpha\beta}+\frac{4\pi i}{\omega}\sigma_{\alpha\beta}(\omega). \qquad (4)$$

The optical conductivity tensor, or equivalently, the dielectric tensor is the important spectral quantity needed for the evaluation of the Kerr effect.[5] The optical conductivity can be computed from the energy band structure by means of the Kubo-Greenwood[11] linear-response expression:[13]

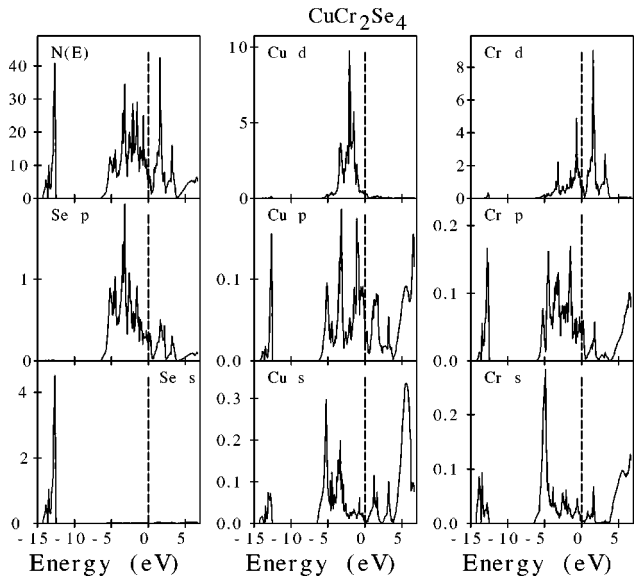

FIG. 2. Fully relativistic, spin-polarized partial densities of states calculated for $CuCr_2Se_4$.

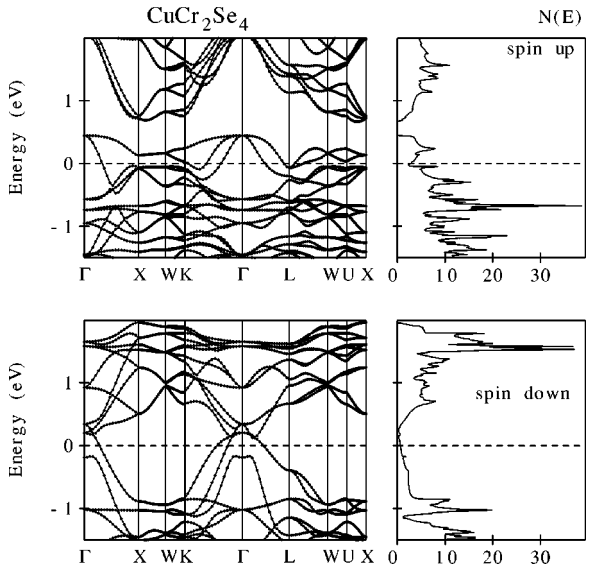

FIG. 3. Spin-projected semirelativistic (without SO interaction) energy band structure and total DOS [in states/(unit cell eV spin)] of $CuCr_2Se_4$.

$$\sigma_{\alpha\beta}(\omega)=\frac{-ie^2}{m^2\hbar V_{uc}}\sum_{\mathbf{k}}\sum_{nn'}\frac{f(\epsilon_{n\mathbf{k}})-f(\epsilon_{n'\mathbf{k}})}{\omega_{nn'}(\mathbf{k})}\times\frac{\Pi^{\alpha}_{n'n}(\mathbf{k})\Pi^{\beta}_{nn'}(\mathbf{k})}{\omega-\omega_{nn'}(\mathbf{k})+i\gamma}, \qquad (5)$$

with $f(\epsilon_{n\mathbf{k}})$ the Fermi function, $\hbar\omega_{nn'}(\mathbf{k})\equiv\epsilon_{n\mathbf{k}}-\epsilon_{n'\mathbf{k}}$, the energy difference of the Kohn-Sham energies $\epsilon_{n\mathbf{k}}$, and γ is the lifetime parameter, which is included to describe the fi-

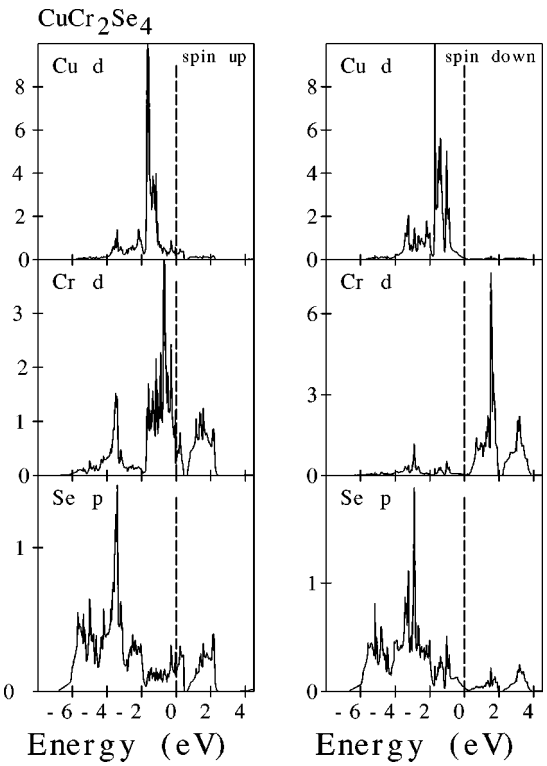

FIG. 4. Spin-projected semirelativistic partial DOS [in states/(atom eV spin)] of $CuCr_2Se_4$.

TABLE I. The experimental and calculated spin and orbital magnetic moments (in μ_B) of $CuCr_2X_4$ compounds. The experimental data for $CuCr_2S_4$ are from Ref. 46, and for $CuCr_2Se_4$ and $CuCr_2Te_4$ from Ref. 47.

Compound	Atom	Ref. 32	M_s	M_l	M_{total}	Expt.
$CuCr_2S_4$	Cu	−0.32	−0.078	−0.011	−0.089	−0.07±0.02
	Cr	3.25	2.679	−0.027	2.652	2.64±0.04
	S	−0.27	−0.098	−0.001	−0.099	−0.05±0.11
$CuCr_2Se_4$	Cu	−0.26	−0.073	−0.009	−0.082	0.01±0.13
	Cr	3.54	2.833	−0.009	2.824	2.81±0.11
	Se	−0.36	−0.137	−0.005	−0.142	−0.25±0.14
$CuCr_2Te_4$	Cu	−0.19	−0.096	−0.006	−0.102	0.05±0.14
	Cr	3.74	3.166	0.021	3.187	3.11±0.16
	Te	−0.48	−0.202	−0.011	−0.213	−0.25±0.14

nite lifetime of excited Bloch electron states. The $\Pi^{\alpha}_{nn'}$ are the dipole optical transition matrix elements, which in a fully relativistic description are given by

$$\mathbf{\Pi}_{nn'}(\mathbf{k}) = m\langle \psi_{n\mathbf{k}} | c\boldsymbol{\alpha} | \psi_{n'\mathbf{k}} \rangle, \tag{6}$$

with $\psi_{n\mathbf{k}}$ the four-component Bloch electron wave function. A detailed description of the optical matrix elements in the Dirac representation is given in Ref. 41.

Equation (5) for the conductivity contains a double sum over all energy bands, which naturally separates into the so-called interband contribution, i.e., $n \neq n'$, and the intraband contribution, $n = n'$. The intraband contribution to the diagonal components of $\boldsymbol{\sigma}$ may be rewritten for zero temperature as

$$\sigma_{\alpha\alpha}(\omega) \equiv \frac{(\omega_{p,\alpha})^2}{4\pi} \frac{i}{\omega + i\gamma_D}, \tag{7}$$

with $\omega_{p,\alpha}$ the components of the plasma frequency, which are given by

$$(\omega_{p,\alpha})^2 \equiv \frac{4\pi e^2}{m^2 V_{uc}} \sum_{n\mathbf{k}} \delta(\epsilon_{n\mathbf{k}} - E_F) |\Pi^{\alpha}_{nn}|^2, \tag{8}$$

and E_F is the Fermi energy. For cubic symmetry, we furthermore have $\omega_p^2 \equiv \omega_{p,x}^2 = \omega_{p,y}^2 = \omega_{p,z}^2$. Equation (7) is identical to the classical Drude result for the ac conductivity, with $\gamma_D = 1/\tau_D$, and τ_D the phenomenological Drude electron relaxation time. The intraband relaxation time parameter γ_D may be different from the interband relaxation time parameter γ. The latter can be frequency dependent,[40] and, because excited states always have a finite lifetime, will be nonzero, whereas γ_D will approach zero for very pure materials. Here we adopt the perfect crystal approximation, i.e., $\gamma_D \rightarrow 0$. For the interband relaxation parameter, on the other hand, we shall use, unless stated otherwise, $\gamma = 0.2$ eV. This value has been found to be on average a good estimate of this phenomenological parameter. The contribution of intraband transitions to the off-diagonal conductivity usually is not considered. Also we did not study the influence of local field effects on the MO properties.

We mention, lastly, that we have calculated the absorptive part of the optical conductivity in a wide energy range (up to 50 eV). The Kramers-Kronig transformation has been used to calculate the dispersive parts of the optical conductivity from the absorptive parts.

IV. CRYSTAL STRUCTURE AND COMPUTATIONAL DETAILS

The chromium spinels $CuCr_2X_4$ (X=S, Se, Te) crystallize in the face-centered cubic (FCC) structure with *two* formula units per *primitive* cell. The space group is $Fm\bar{3}m$ (No. 227) with Cu at the 8*a* positions, Cr at the 16*d* positions, and *X* at the 32*e* positions. In our band structure calculations we used the experimentally measured crystal structures and lattice constants (9.820, 10.327, and 11.140 Å for $CuCr_2S_4$, $CuCr_2Se_4$, and $CuCr_2Te_4$, respectively[42]).

The electronic structure of the compounds was calculated self-consistently using the local spin density approximation[43] and the fully relativistic LMTO method[39] in the atomic-sphere approximation, including the combined correction (ASA+CC).[44] The spin polarization has been included in the variational step.[36] The combined correction terms have been included also in calculation of the optical matrix elements. To improve the potential we include three additional empty spheres in the 8*b*, 16*c*, and 48*f* positions. The radii of the overlapping spheres were $s_{\text{Cu}} = 2.1577$, $s_{\text{Cr}} = 2.2863$, s_{Se}

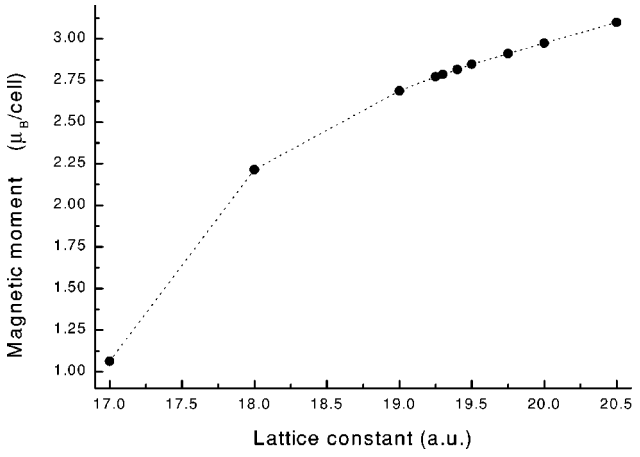

FIG. 5. Lattice constant dependence of the magnetic moment per Cr site calculated for $CuCr_2Se_4$.

TABLE II. The centers of gravity E_ν relative to the Fermi energy (in eV) in $CuCr_2X_4$ compounds.

Compound	Cu $d_{3/2}$	Cu $d_{5/2}$	Cr $d_{3/2}$	Cr $d_{5/2}$	X $p_{1/2}$	X $p_{3/2}$
$CuCr_2S_4$	−2.42	−2.13	0.21	0.30	−2.87	−2.76
$CuCr_2Se_4$	−2.37	−2.08	0.26	0.35	−2.94	−2.49
$CuCr_2Te_4$	−3.24	−2.95	0.04	0.13	−2.45	−1.21

$=2.4954$, $s_{E1}=2.0674$, $s_{E2}=1.8465$, and $s_{E3}=1.4817$ a.u.

The basis consisted of the Cu and Cr s, p, d, and f; Se s,p, and d, and empty spheres s, and p LMTO's. The energy expansion parameters $E_{\nu Rl}$ were chosen at the centers of gravity of the occupied parts of the partial state densities both for charge density calculations and for MO calculations.

The **k**-space integrations were performed with the improved tetrahedron method[45] and charge self-consistently was obtained with 480 irreducible **k** points.

V. RESULTS AND DISCUSSION

The fully relativistic spin-polarized energy band structure of ferromagnetic $CuCr_2Se_4$, shown in Fig. 1, is rather complicated. It may, however, be understood from the total and partial density of states (DOS) presented in Fig. 2. The occupied part of the band structure can be subdivided into two regions separated by an energy gap of about 6 eV. The bands in the lowest region have mostly a Se s character with some amount of Cu and Cr sp character mixed in. The highest region can be characterized as a bonding combination of Cu and Cr d and Se p states. This complex is separated from the antibonding states by a pseudogap around the Fermi level. The antibonding states are created mostly by the Cr d states. Another pseudogap arises above the Cr d band at about 4 eV above the Fermi energy. Figure 3 shows the semirelativistic (without SO interaction) spin-polarized energy band structure and total DOS's of the up- and down-spin bands of ferromagnetic $CuCr_2Se_4$. It is seen that the pseudogap around the Fermi level originates from the minority spin valence bands. Figure 4 shows the semirelativistic spin-polarized Cu and Cr d and Se p partial DOS's. Cu d minority spin valence bands are fully occupied and almost occupied for the majority spin producing a very small negative magnetic moment at Cu (see Table I). The orbital magnetic moment is rather small for all three atoms due to small SO coupling. The calculated spin polarization of the Cr $3d$ electrons is 2.824 μ_B and agrees well with the experimental value obtained by Colominas[47] using polarized neutron diffraction measurements (2.81 ± 0.11 μ_B). Theoretical net magnetization per formula unit $CuCr_2Se_4$ is equal to 5.282 μ_B. We also performed lattice constant optimization for $CuCr_2Se_4$. The theoretically optimized lattice constant deviates from the experimental one by less than 1%. The consideration of gradient corrections changes this result insignificantly. The lattice constant dependence of magnetization is shown on Fig. 5. Magnetic structure and magnetic moments near the equilibrium volume are stable and only under abnormal pressure when $\Delta a=2$ a.u. are the moments at the Cr site decreasing rapidly. The total energy difference between FM and AFM phase at equilibrium volume is close to 800 K.

The main trend in the electronic structure of the sequence of $CuCr_2X_4$ compounds ($X=$S, Se, Te) results from the characteristic trend in the chalcogenide p wave functions and from the systematic change of the lattice parameters. The counteraction of screening by inner atomic shells and of relativistic effects leads to the characteristic trend in the position of the atomic p state and hence of the center of gravity of the chalcogenide p band (Table II). The SO splitting of Cu d

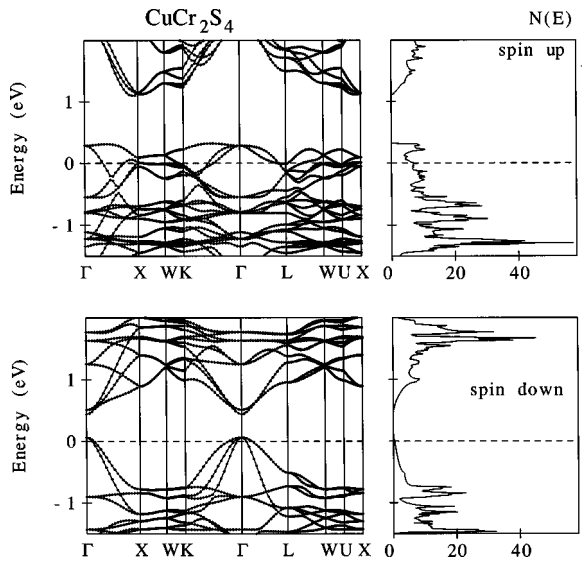

FIG. 6. Spin-projected semirelativistic energy band structure and total DOS [in states/(unit cell eV spin)] of $CuCr_2S_4$.

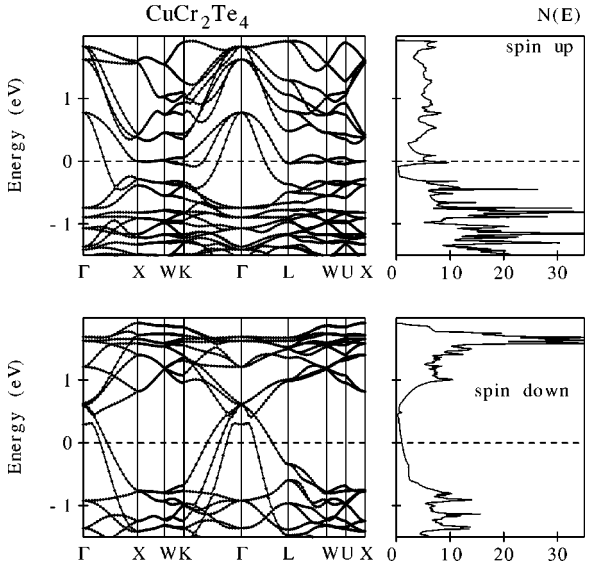

FIG. 7. Spin-projected semirelativistic energy band structure and total DOS [in states/(unit cell eV spin)] of $CuCr_2Te_4$.

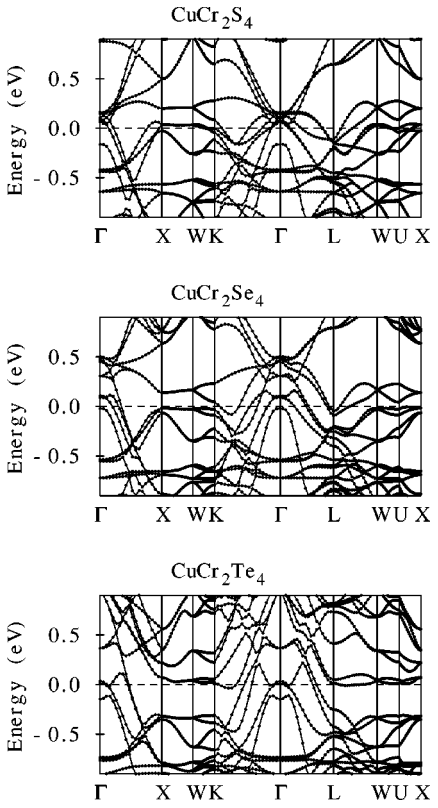

FIG. 8. Relativistic, spin-polarized energy band structures of $CuCr_2X_4$.

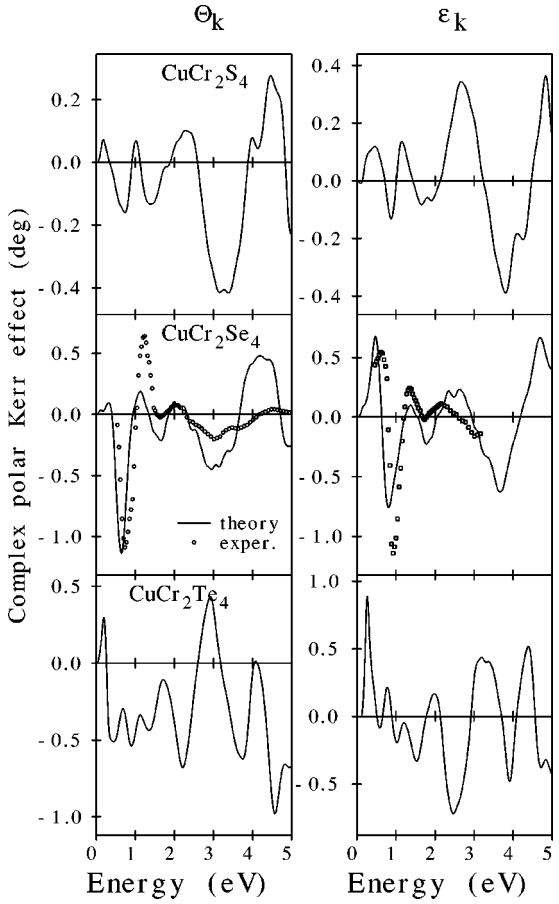

FIG. 9. Calculated and experimental Kerr rotation (θ_K) and Kerr ellipticity (ε_K) spectra of the $CuCr_2X_4$ compounds. The experimental data are those of Ref. 28.

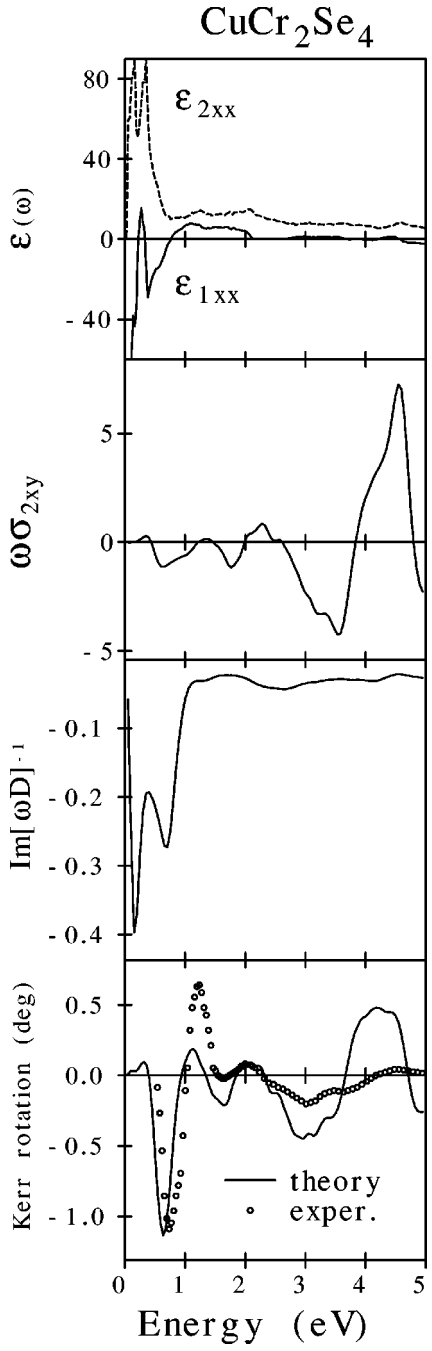

FIG. 10. Decomposition of the Kerr rotation spectrum of $CuCr_2Se_4$ into separate contributions. Top panel: calculated real and imaginary part of the diagonal dielectric function, ε_{1xx}, and ε_{2xx}. Third panel from the top: the imaginary part of $[\omega D]^{-1}$ which results from ε_{1xx} and ε_{2xx}. Bottom panel: the Kerr rotation which results from a combination of $\mathrm{Im}[\omega D]^{-1}$ and $\omega\sigma_{2xy}$ (second panel from the top in 10^{20} s^{-2}). The experimental Kerr angle spectrum is after Ref. 28.

center of gravity is equal 0.29 eV. For Cr *d* states this value is smaller and equal to 0.09 eV for all three compounds. But SO splitting for chalcogenide *p* states shows one order of magnitude increase from S (0.11 eV) to Te (1.24 eV). The *p* bandwidth is monotonically increasing from S to Te due to the increasing extension of the atomic wave function, although the lattice constant increases too. The increasing of the lattice constant from S to Te leads to the monotonic

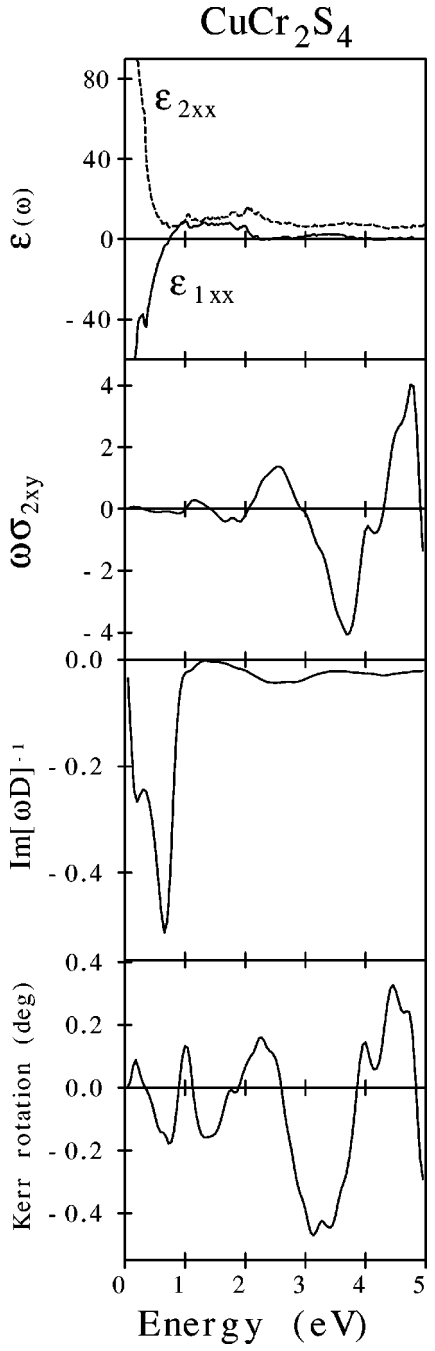

FIG. 11. Same as in Fig. 10, but for $CuCr_2S_4$.

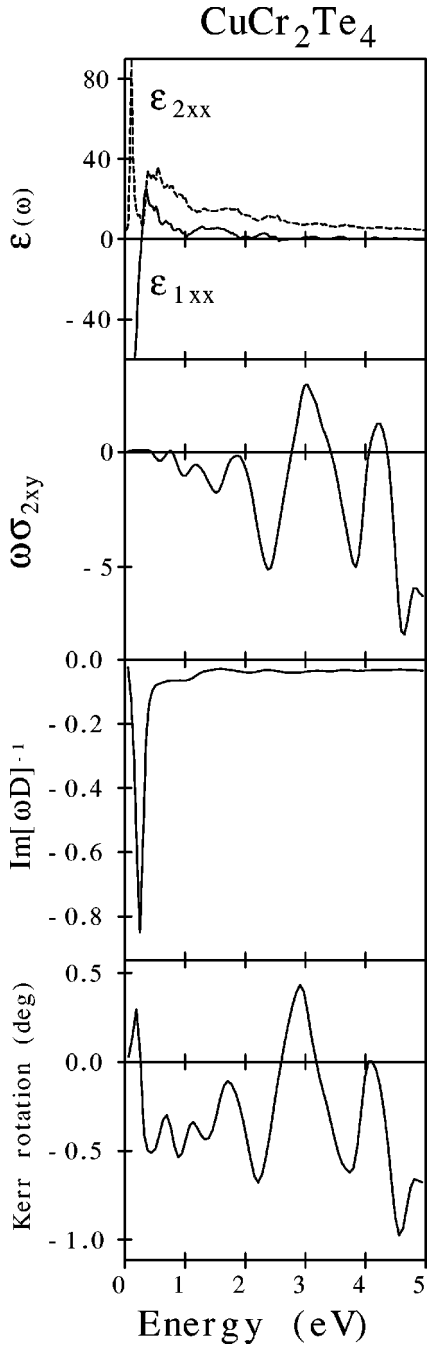

FIG. 12. Same as in Fig. 10, but for $CuCr_2Te_4$.

increase of the spin polarization of the Cr 3*d* electrons (see Table I).

A previous band structure calculation for $CuCr_2Se_4$ used the discrete-variational X_α method and proposed this compound to be half-metallic with a gap of about 0.4 eV for the spin-down bands. The prediction of half-metallicity was based on nonrelativistic band structure calculations. This approximation is often acceptable for the study of certain material properties, but especially for the investigation of MO properties it is not, because the Kerr effect is a purely relativistic effect. Semirelativistic LMTO band structure calculations for $CuCr_2S_4$ produce a direct gap in the minority energy bands of about 0.4 eV, but slightly above the Fermi level at 0.05 to 0.45 eV (see Fig. 6). There is another indirect energy gap for the majority energy bands at 0.3 to 1.09 eV (Fig. 6). There is still an indirect energy gap in $CuCr_2Se_4$ but only for the majority bands above the Fermi energy (Fig. 3). There is not any gap in the $CuCr_2Te_4$ compound for either spin direction (Fig. 7). The inclusion of SO interaction in the energy band calculations destroys the gaps in both the $CuCr_2S_4$ and $CuCr_2Se_4$ compounds (Fig. 8).

After the consideration of the above band structure properties we turn to the MO spectra. In Fig. 9 we show the calculated and experimental[28] MO Kerr spectra of the three isoelectronic $CuCr_2X_4$ compounds. There exists rather good agreement between the experimental Kerr spectra and the *ab initio* calculated one for $CuCr_2Se_4$. Overall, the experimental features are reasonably well reproduced, except for the magnitude of the second Kerr rotation peak of $CuCr_2Se_4$, for which theory predicts smaller values than are

experimentally observed. There is also a small energy shift by about 0.1 eV in the position of the main Kerr rotation and ellipticity peaks in $CuCr_2Se_4$. We can conclude, therefore, that the anomalous behavior of the MO Kerr spectra in $CuCr_2Se_4$ is well described by band structure theory.

To investigate the origin of the Kerr spectra, we consider the separate contributions of both the numerator of Eq. (3), i.e., $\sigma_{xy}(\omega)$ and the denominator, $D(\omega) \equiv \sigma_{xx}[1 + (4\pi i/\omega)\sigma_{xx}]^{1/2}$. In Fig. 10 we show how the separate contributions of numerator and denominator bring about the Kerr angle of $CuCr_2Se_4$. The imaginary part of the inverse denominator (times the photon frequency), $\mathrm{Im}[\omega D]^{-1}$, displays a double resonance structure at about 0.14 and 0.7 eV. The imaginary part of $\omega\sigma_{xy}$, i.e., $\omega\sigma_{2xy}$ displays a very small value at 0.14 eV and a reasonable size minima at 0.7 eV. Therefore the first peak in the Kerr rotation at 0.65 eV results as a combination of a deep resonance structure of the denominator and interband transitions contributing into σ_{2xy}. The nature of the peaks in $\mathrm{Im}[\omega D]^{-1}$ can be understood from the top panel in Fig. 10, where the complex diagonal dielectric function is shown: its real part, ε_{1xx}, crosses the energy axis at about 0.2 and 0.75 eV, and its imaginary part, ε_{2xx}, has a shallow minima at the same energies. The second and others peaks in the Kerr rotation of $CuCr_2Se_4$ at 1.2, 2.1, 3.0, and 4.5 eV, are coming from the corresponding maxima in $\omega\sigma_{2xy}$, which in turn are known to be due to the interplay of SO coupling and spin polarization.

Next, we consider the spectra for the compound $CuCr_2S_4$ in more detail, which is shown in Fig. 11. In this compound the inverse denominator $\mathrm{Im}[\omega D]^{-1}$ again displays a strong resonance at 0.7 eV, which is even larger than that for $CuCr_2Se_4$. The reason for the calculated resonance in the inverse denominator lies again in the frequency dependence of the diagonal dielectric function, which is shown in the top panel of Fig. 11. However, the off-diagonal conductivity $\omega\sigma_{2xy}$ for $CuCr_2S_4$ is much smaller in that energy interval than that of $CuCr_2Se_4$, in accordance with the smaller SO coupling on S. The resulting Kerr rotation has a much smaller peak of $-0.2°$ (see Fig. 11).

In Fig. 12 we show the spectral quantities for $CuCr_2Te_4$. $\omega\sigma_{2xy}$ is larger than that of $CuCr_2S_4$ and $CuCr_2Se_4$ in the energy range 1–5 eV. This is simply due to the larger SO interaction of Te as compared to that of S and Se. The inverse denominator $\mathrm{Im}[\omega D]^{-1}$ exhibits a strong resonance at very small energy, about 0.2 eV, which is much larger than that for $CuCr_2S_4$ and $CuCr_2Se_4$, but such a strong resonance does not lead to a large Kerr rotation due to lack of the interband transitions in this energy region. Almost all the spectral shape of the Kerr rotation in the $CuCr_2Te_4$ compound (except for the first peak at about 0.3 eV) is determined by $\omega\sigma_{2xy}$.

The calculated plasma frequencies evaluated using Eq. (8) in the compounds are very small, $\hbar\omega_p = 1.62$, 1.45, and 1.60 eV for $CuCr_2Se_4$, $CuCr_2Se_4$, and $CuCr_2Te_4$, respectively.

VI. SUMMARY

The origin of large Kerr angle in $CuCr_2Se_4$ as compared to the Kerr angles in $CuCr_2S_4$ and $CuCr_2Te_4$ can be completely understood from our calculations. In these three compounds, first, the off-diagonal conductivities $\sigma_{xy}(\omega)$ are quite different, which is a direct result of the different relativistic electronic structures. Their $\omega\sigma_{2xy}$ spectra are distinctly different, while, on the other hand, the $\omega\sigma_{2xy}$ of $CuCr_2Se_4$ and $CuCr_2S_4$ have a similar structure, but not a similar magnitude (see Figs. 10 and 11). There is also the influence of the denominators as exemplified in $\mathrm{Im}[\omega D]^{-1}$. These are similar in shape and magnitude for $CuCr_2Se_4$ and $CuCr_2S_4$, but the magnitude of $\mathrm{Im}[\omega D]^{-1}$ in $CuCr_2S_4$ is larger.

In conclusion, we find that the Kerr spectra of $CuCr_2S_4$, $CuCr_2Se_4$, and $CuCr_2Te_4$ can be described by using electronic structure calculations within the LSDA. The puzzling anomalities in the Kerr spectra of these compounds arise from an interplay of compound related differences in the SO interaction and also in relative positions of energy bands.

ACKNOWLEDGMENTS

This work was carried out at the Ames Laboratory, which is operated for the U.S. Department of Energy by Iowa State University under Contract No. W-7405-82. This work was supported by the Director for Energy Research, Office of Basic Energy Sciences of the U.S. Department of Energy.

*Permanent address: Institute of Metal Physics, 36 Vernadskii str., 252142 Kiev, Ukraine.

[1] J. Kerr, Philos. Mag. **3**, 321 (1877).

[2] C.D. Mee and E.D. Daniel, *Magnetic Recording* (McGraw-Hill, New York, 1987); M. Mansuripur, *The Physical Principles of Magneto-Optical Recording* (Cambridge University Press, Cambridge, England, 1995).

[3] K.H.J. Buschow, in *Ferromagnetic Materials*, edited by E.P. Wohlfarth and K.H.J. Buschow (North-Holland, Amsterdam, 1988), Vol. 4, p. 588.

[4] W. Reim and J. Schoenes, in *Ferromagnetic Materials*, edited by E.P. Wohlfarth and K.H.J. Buschow (North-Holland, Amsterdam, 1990), Vol. 5, p. 133.

[5] J. Schoenes, in *Materials Science and Technology, Vol. 3A*: *Electronic and Magnetic Properties of Metals and Ceramics* (volume editor: K.H.J. Buschow), edited by R. W. Cahn, P. Haasen, and E.J. Kramer (Verlag Chemie, Weinheim, 1992), p. 147.

[6] H.R. Hulme, Proc. R. Soc. London, Ser. A **135**, 237 (1932).

[7] C. Kittel, Phys. Rev. **83**, 208 (1951).

[8] P.N. Argyres, Phys. Rev. **97**, 334 (1955).

[9] B.R. Cooper, Phys. Rev. **139**, A1504 (1965).

[10] G.S. Krinchik and E.A. Gan'shina, Zh. Éksp. Teor. Fiz. **65**, 1970 (1973) [Sov. Phys. JETP **38**, 983 (1974)].

[11] R. Kubo, J. Phys. Soc. Jpn. **12**, 570 (1957).

[12] A.E. Kondorsky and A.V. Vediaev, J. Appl. Phys. **39**, 559 (1968).

[13] C.S. Wang and J. Callaway, Phys. Rev. B **9**, 4897 (1974).

[14] G.H.O. Daalderop, F.M. Mueller, R.C. Albers, and A.M. Boring, J. Magn. Magn. Mater. **74**, 211 (1988); H. Ebert, P. Strange, and B.L. Gyorffy, J. Phys. (Paris) Colloq. **8**, 31 (1988); Yu. Uspenskii and S.V. Halilov, Zh. Éksp. Teor. Fiz. **95**, 1022 (1989) [Sov. Phys. JETP **68**, 588 (1989)].

[15] E.T. Kulatov, Yu.A. Uspenskii, and S.V. Khalilov, Phys. Lett. A **195**, 267 (1994); Yu.A. Uspenskii, E.T. Kulatov, and S.V. Khalilov, Zh. Éksp. Teor. Fiz. **107**, 1708 (1995) [JETP **80**, 952

(1995)]; Yu.A. Uspenskii, E.T. Kulatov, and S.V. Khalilov, Phys. Rev. B **54**, 474 (1996); E.T. Kulatov, Yu.A. Uspenski, and S.V. Khalilov, Fiz. Tverd. Tela (St. Petersburg) **38**, 3066 (1996) [Phys. Solid State **38**, 1677 (1996)].

[16] P.M. Oppeneer, J. Sticht, and F. Herman, J. Magn. Soc. Jpn. **15**, S1, 73 (1991); P.M. Oppeneer, T. Maurer, J. Sticht, and J. Kübler, Phys. Rev. B **45**, 10 924 (1992); I. Osterloch, P.M. Oppeneer, J. Sticht, and J. Kübler, J. Phys.: Condens. Matter **6**, 285 (1994); J. Köhler, L. Sandratskii, and J. Kübler, Physica B **253**, 272 (1998).

[17] V.N. Antonov, A.Ya. Perlov, A.P. Shpak, and A.N. Yaresko, J. Magn. Magn. Mater. **146**, 205 (1995); P.M. Oppeneer and V.N. Antonov, in *Spin-Orbit Influenced Spectroscopies of Magnetic Solids*, edited by H. Ebert and G. Schütz (Springer, Berlin, 1996), p. 29; P.M. Oppeneer, M.S.S. Brooks, V.N. Antonov, T. Kraft, and H. Eschrig, Phys. Rev. B **53**, R10 437 (1996); P.M. Oppeneer, V.N. Antonov, A.Ya. Perlov, A.N. Yaresko, T. Kraft, and H. Eschrig, Physica B **230-232**, 544 (1997).

[18] S.P. Lim, D.L. Price, and B.R. Cooper, IEEE Trans. Magn. **27**, 3648 (1991); B.R. Cooper, S.P. Lim, and I. Avgin, J. Phys. Chem. Solids **56**, 1518 (1995).

[19] X. Wang, V.P. Antropov, and B.N. Harmon, IEEE Trans. Magn. **30**, 4458 (1994); V.P. Antropov, A.I. Lichtenstein, and B.N. Harmon, J. Magn. Magn. Mater. **140**, 1161 (1995); B.N. Harmon, V.P. Antropov, A.I. Liechtenstein, I.V. Soloviev, and V.I. Anisimov, J. Phys. Chem. Solids **56**, 1521 (1995); Yu.A. Uspenskii, V.P. Antropov, and B.N. Harmon, Phys. Rev. B **56**, R11 396 (1997).

[20] S.V. Halilov and R. Feder, Solid State Commun. **88**, 749 (1993); S. Uba, L. Uba, A.Ya. Perlov, A.N. Yaresko, V.N. Antonov, and R. Gontarz, J. Phys.: Condens. Matter **9**, 447 (1997); H. Ebert, A.Ya. Perlov, A.N. Yaresko, V.N. Antonov, and S. Uba, in *Magnetic Ultrathin Films, Multilayers and Surfaces - 1997*, edited by J. Tobin *et al.* (MRS, Pittsburgh, PA, 1997), p. 407.

[21] A.I. Lichtenstein, V.P. Antropov, and B.N. Harmon, Phys. Rev. B **49**, 10 770 (1995).

[22] A.N. Yaresko, P.M. Oppeneer, A.Ya. Perlov, V.N. Antonov, T. Kraft, and H. Eschrig, Europhys. Lett. **36**, 551 (1996).

[23] P.G. van Engen, K.H.J. Buschow, R. Jongebreur, and M. Erman, Appl. Phys. Lett. **42**, 202 (1983); P.G. van Engen, K.H.J. Buschow, and M. Erman, J. Magn. Magn. Mater. **30**, 374 (1983); P. G. van Engen, Ph.D. thesis, Technical University Delft, 1983; R.A. de Groot, F.M. Mueller, P.G. van Engen, and K.H.J. Buschow, Phys. Rev. Lett. **50**, 2024 (1983).

[24] V.N. Antonov, P.M. Oppeneer, A.N. Yaresko, A.Ya. Perlov, and T. Kraft, Phys. Rev. B **56**, 13 012 (1997).

[25] I. Nacatani, H. Nose, and K. Masumoto, J. Phys. Chem. Solids **39**, 743 (1978).

[26] H. Hahn, C. de Lorentn, and B. Harder, Z. Anorg. Allg. Chem. **283**, 138 (1956).

[27] F. K. Lotgering, in *Proceedings of the International Conference on Magnetism, Nottingham, 1964* (The Institute of Physics and the Physical Society, London, 1965), p. 533.

[28] H. Brandle, J. Schoenes, P. Wachter, and F. Hulliger, Appl. Phys. Lett. **56**, 2602 (1990).

[29] F.K. Lotgering and R.P. van Stapele, J. Appl. Phys. **39**, 417 (1968).

[30] J.B. Goodenough, Solid State Commun. **5**, 577 (1967).

[31] J.I. Horikawa, T. Hamajima, F. Ogata, T. Kambara, and K.I. Gondaira, J. Phys. C **15**, 2613 (1982).

[32] F. Ogata, T. Hamajima, T. Kambara, and K.I. Gondaira, J. Phys. C **15**, 3483 (1982).

[33] W.H. Kleiner, Phys. Rev. **142**, 318 (1966).

[34] A.H. MacDonald and S.H. Vosko, J. Phys. C **12**, 2977 (1979).

[35] H. Ebert, H. Freyer, A. Vernes, and G.-Y. Guo, Phys. Rev. B **53**, 7721 (1996).

[36] H. Ebert, Phys. Rev. B **38**, 9390 (1988).

[37] I.V. Solovyev, A.B. Shik, V.P. Antropov, A.I. Liechtenstein, V.A. Gubanov, and O.K. Andersen, Fiz. Tverd. Tela (Leningrad) **31**, 13 (1989) [Sov. Phys. Solid State **31**, 1285 (1989)].

[38] O.K. Andersen, Phys. Rev. B **12**, 3060 (1975); D.D. Koelling and B.N. Harmon, J. Phys. C **10**, 3107 (1977).

[39] V.V. Nemoshkalenko, A.E. Krasovskii, V.N. Antonov, Vl.N. Antonov, U. Fleck, H. Wonn, and P. Ziesche, Phys. Status Solidi B **120**, 283 (1983).

[40] A. Santoni and F.J. Himpsel, Phys. Rev. B **43**, 1305 (1991).

[41] V.N. Antonov, A.I. Bagljuk, A.Ya. Perlov, V.V. Nemoshkalenko, Vl.N. Antonov, O.K. Andersen, and O. Jepsen, Low Temp. Phys. **19**, 494 (1993).

[42] P. Villars and L. D. Calvert, *Pearson's Handbook of Crystallographic Data for Intermetallic Phases* (ASM International, Materials Park, OH, 1991).

[43] U. von Barth and L.A. Hedin, J. Phys. C **5**, 1692 (1972).

[44] V. V. Nemoshkalenko and V. N. Antonov, *Computational Methods in Solid State Physics* (Gordon and Breach, London, 1998).

[45] P.E. Blöchl, O. Jepsen, and O.K. Andersen, Phys. Rev. B **49**, 16 223 (1994).

[46] O. Yamashita, Y. Yamaguchi, I. Nakatani, H. Watanabe, and K. Masumoto, J. Phys. Soc. Jpn. **46**, 1146 (1979).

[47] C. Colominas, Phys. Rev. **153**, 558 (1967).